JOURNAL OF GUIDANCE, CONTROL, AND DYNAMICS
Vol. 30, No. 1, January–February 2007

Cyclic Spacecraft Formations: Relative Motion Control Using Line-of-Sight Measurements Only

Pini Gurfil*
Technion—Israel Institute of Technology, Haifa 32000, Israel
and
David Mishne†
Rafael, Ltd., Haifa 31021, Israel

DOI: 10.2514/1.19850

In this paper, we develop a new nonlinear relative spacecraft motion control law based on line-of-sight measurements only. Each spacecraft tracks its neighboring spacecraft to produce a line-of-sight vector measurement, and the last spacecraft tracks again the first spacecraft to create a cyclic formation. We show that cyclic leaderless formations controlled by line-of-sight measurements only are stable in the sense of energy matching. The initial semimajor axis errors relative to a reference semimajor axis all tend to the same value, which is the centroid of the initial semimajor axis errors. The stable behavior is achieved by using both full line-of-sight feedback (range and bearing) and partial line-of-sight feedback (bearing only). We also investigate the case of leader formations, where a designated leader does not track any other spacecraft. In this case, the semimajor axes of all follower spacecraft will converge to the initial semimajor axis of the leader. We also discuss an intermediate case, in which only part of the spacecraft forms a cycle. In this case, the cyclic formation members will determine the semimajor axes of all the other, noncyclic, spacecraft. We use elementary graph theory to describe the resulting formation topologies and conclude the development with an illustrating example.

Nomenclature

A	=	system matrix
a	=	semimajor axis
C^N	=	cycle of N vertices
e	=	eccentricity
$\boldsymbol{f}$	=	specific force control vector
f_t	=	tangential force of control vector
G	=	graph
K	=	control gain
$\mathcal{L}$	=	Euler–Hill reference frame
ℓ	=	line-of-sight vector
N	=	number of spacecraft
n	=	mean motion
S_i	=	spacecraft i
T	=	orbital period of reference orbit
$\boldsymbol{V}$	=	velocity vector
v	=	graph vertex
x, y, z	=	position components
$\Delta(\cdot)$	=	variation of $(\cdot)$
ε	=	total energy
Λ	=	eigenvalue matrix
λ	=	eigenvalue
μ	=	gravitational constant
$\boldsymbol{\rho}$	=	position vector in Euler–Hill frame
Φ	=	transition matrix

Subscripts

$(\cdot)_{eq}$	=	equilibrium value
$(\cdot)_i$	=	value of $(\cdot)$ for spacecraft i
$(\cdot)_{ref}$	=	reference value
$(\cdot)_{ss}$	=	steady-state value

Received 2 September 2005; revision received 3 September 2006; accepted for publication 14 September 2006.

*Senior Lecturer, Faculty of Aerospace Engineering; pgurfil@technion.ac.il. Associate Fellow AIAA.

†Chief Systems Engineer, Space Systems Directorate; davidm@rafael.co.il. Associate Fellow AIAA.

I. Introduction

CONTROL of relative spacecraft motion is an enabling technology for spacecraft formation flying (FF) missions, which constitute a significant share of future space projects. Relative motion control approaches can be roughly categorized into two main branches: impulsive control, relying on chemical thrusters, and continuous control, using low-thrust electric propulsion. Impulsive formation keeping assumes that the orbital elements of some reference orbit (which could be an orbit of the actual formation leader) are known and attempts to generate control commands which will match the instantaneous orbital elements to those of the desired values [1], even under orbital perturbations [2]. Alternatively, recent impulsive formation keeping approaches have advocated the use of the Cartesian relative spacecraft position components [3] or hybrid classical elements-relative position feedback [4].

Continuous control approaches have mostly used full-state feedback of the Cartesian relative position and velocity to develop high-precision tracking control laws, capable of maintaining small steady-state errors under a myriad of orbital perturbations. In this regard, most of the modern control paradigms, including neural-adaptive control [5], differential-geometric methods [6], linear time-varying optimizing control [7], and linear matrix inequalities-based control [8] have been attempted. However, only a few studies have taken into account the measurement hardware required for implementing FF missions. Most of these works advocated the use of global positioning system (GPS)-based relative position sensors for controlling Earth-centered FF missions and GPS-like pseudolite systems for beyond-GPS-range missions (cf. [9] and references therein).

However, in many practical cases, GPS is of questionable value for precision formation flying missions beyond low Earth orbits. Moreover, in some scenarios there is no infrastructure for full collaboration and communication among the formation satellites. These two arguments necessitate finding an alternative to GPS-based formation flying.

In this work, we propose a different approach. We show that knowledge of all relative position components is unnecessary to achieve bounded formations; in fact, only the relative line of sight (LOS) between two spacecraft is required to achieve stable FF. Moreover, we show that even the relative range is unnecessary; stable formations can be achieved by measuring the LOS bearing only. Such measurements can be acquired by several readily available methods, such as the use of vision-based sensors that combine star trackers and optical/RF ranging [10] or a combination of onboard optical tracking with rate gyros for the determination of the inertial LOS. In any case, only the relative LOS vector is required for the control; there is no need to measure the absolute position of each satellite.

The LOS-based FF control approach requires that each spacecraft in the formation tracks some other spacecraft in order to generate a LOS measurement. Suppose that each spacecraft tracks the LOS to some neighboring (e.g., the closest) spacecraft and the first spacecraft tracks again the last spacecraft so as to create a cycle. This topology gives rise to the concept of cyclic spacecraft formations, a newly developed branch of the classical problem of cyclic pursuit [11–13], described as follows: consider N agents which are initially placed at some arbitrary positions. Each agent attempts to intercept a single neighboring agent. What will the final configuration of this multiagent system be?

In this paper, we adapt the cyclic pursuit problem to the FF case and pose the following problem: Assume that there are N spacecraft, with each spacecraft measuring the LOS to a single neighboring spacecraft, and the last spacecraft tracks the first spacecraft. Is the resulting formation stable in the sense of energy matching? [3]

We show that indeed, the LOS-based control law implemented using a cyclic topology renders stable formations. This holds true both for the full, active, LOS measurement (range and bearing) and reduced, passive, LOS measurement (bearing only). Moreover, we also implement the LOS-based control formalism on noncyclic (i.e., leader) formations and partially cyclic formations and show that stable formations are achieved. However, cyclic formations are preferable due to two main reasons: 1) cyclic formations are inherently leaderless, and are hence more robust; and 2) cyclic control steers the formation toward the centroid of the initial semimajor axes (SMAs). On the other hand, spacecraft in noncyclic (i.e., leader based) formations tend to equalize their SMAs to that of the leader. Finally, we prove that if there exists a cycle in the formation which includes only some of the spacecraft, the other spacecraft will equalize their SMAs to the centroid of the initial SMAs of the spacecraft flying in a cycle. We call these structures tadpole formations.

II. Mathematical Preliminaries

In the following treatment, we shall use elementary graph theory to define the concept of cyclic spacecraft formations. The linearized dynamics of such formations is described by a special class of matrices, called circulant matrices. Therefore, for the establishment of the main ideas of this paper, a few mathematical preliminaries dealing with graph theory and circulant matrices are required. Thus, the following exposition summarizes some pertinent mathematics.

A. Elementary Graph Theory

Throughout our discussion, we shall adopt the terminology used in [14]. The most basic definition of a graph is a pair $G = (V, E)$ of sets such that the elements of E are 2-element subsets of V. The elements of V are the vertices, and the elements of E are the edges. The degree of a vertex v, $d_G(v)$, is the number of edges at v. If all vertices of G have the same degree, then G is regular. A path is a nonempty graph $P = (V, E)$ of the form $V = \{v_1, v_2, \ldots, v_N\}$, $E = \{v_1v_2, v_2v_3, \ldots, v_{N-1}v_N\}$.

If $P = v_1, \ldots, v_Nv_1$ is a path and $N \geq 3$, then the graph P is called a cycle. The length of a cycle is its number of edges (or vertices); a cycle of length m is denoted by C^m. If $m = N$, the cycle is called Hamiltonian.

A directed graph (or digraph) is a pair (V, E) of disjoint sets of vertices and edges together with two maps assigning to every edge ε an initial vertex $\text{init}(\varepsilon)$ and a terminal vertex $\text{ter}(\varepsilon)$. The edge ε is said to be directed from $\text{init}(\varepsilon)$ to $\text{ter}(\varepsilon)$. Consequently, a path is always directed, and hence a cycle is a digraph with $d_G(v) = 2$, where one edge is incident toward and the other is incident away from the vertex v.

Finally, if $P = v_1, \ldots, v_N$ is an acyclic (directed) path with $\text{init}(v_{k-1}v_k) = v_{k-1}$, $(v_{k-1}v_k) = v_k$, and $d_G(v_k) = 1$, then the graph P is called a k-leader graph (or simply a path graph) and is denoted by L^k; the leader graph is a tree, which is an acyclic (directed) graph.

The formalism presented above will be used in the sequel to define the concept of cyclic formations and to describe the dynamics in case of a cycle breakup and the emergence of leader formations.

B. Circulant Matrices

An $n \times n$ circulant matrix has the from [13,15]:

$$C = \begin{bmatrix} c_1 & c_2 & \cdots & c_n \\ c_n & c_1 & \cdots & c_{n-1} \\ \vdots & \vdots & \vdots & \vdots \\ c_2 & c_3 & \cdots & c_1 \end{bmatrix} \triangleq \text{circ}(c_1, c_2, \ldots, c_n) \tag{1}$$

The entire matrix is defined by its first row. Each subsequent row is the row above shifted one element to the right and wrapped around modulo n.

An important property of circulant matrices is their diagonalizability. To show this, define $\omega = e^{2\pi I/n}$, $I = \sqrt{-1}$, and let F be the unitary $n \times n$ Fourier matrix given by

$$F = \frac{1}{\sqrt{n}} \begin{bmatrix} 1 & 1 & 1 & \ldots & 1 \\ 1 & \omega & \omega^2 & \ldots & \omega^{n-1} \\ 1 & \omega^2 & \omega^4 & \ldots & \omega^{2(n-1)} \\ \vdots & \vdots & \vdots & & \vdots \\ 1 & \omega^{n-1} & \omega^{2(n-1)} & \ldots & \omega^{(n-1)(n-1)} \end{bmatrix} \tag{2}$$

with F^* being the conjugate transpose, and $F^*F = I$. It is shown in [15] that a diagonal eigenvalue matrix $\Lambda = \text{diag}(\lambda_1, \lambda_2, \ldots, \lambda_n)$ is produced by the similarity transformation

$$\Lambda = F^*CF \tag{3}$$

so F is, in fact, the eigenvector matrix of C. The eigenvalues are given by

$$\lambda_i = p(\omega^{i-1}), \qquad i = 1, 2, \ldots, n \tag{4}$$

where p is a polynomial called the circulant's representer and is given by [13,15]

$$p(\omega) = c_1 + c_2\omega + c_3\omega^2 + \cdots + c_n\omega^{n-1} \tag{5}$$

We shall use Eqs. (3–5) to prove interesting and useful properties of cyclic spacecraft formations.

III. Cyclic Formation Control Problem Formulation

The study of vehicle formations using graph-theoretic methods has shown much promise [16]. In this paper we study the relative motion control of a group of N spacecraft, S_i, $i = 1, \ldots, N$, flying on elliptic orbits relative to a circular reference orbit to create a formation. We shall treat this spacecraft formation as a digraph F^N and will term it a formation graph, whose edges are the relative position vectors. Each spacecraft S_i constitutes a vertex in F^N.

The dynamic equations of relative motion are obtained via the usual formalism, entailing a transformation of the position vector of each vehicle from an inertial frame to a rotating local-vertical local-horizon Euler–Hill reference frame, $\mathcal{L}$, defined by the unit vectors $\hat{\boldsymbol{x}}$, $\hat{\boldsymbol{y}}$, $\hat{\boldsymbol{z}}$, as shown in Fig. 1. The origin of this coordinate system is set on a circular reference orbit about a primary gravitational body. It is rotating with mean motion n_{ref}, with the reference orbit plane as the

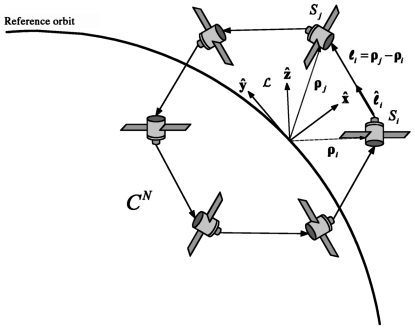

Fig. 1 Hamiltonian cycle: A cyclic formation C^N formed from the digraph F^N in the Euler–Hill reference frame $\mathcal{L}$.

fundamental plane. The positive $\hat{\boldsymbol{x}}$ axis points radially outward, the $\hat{\boldsymbol{y}}$ axis lies on the fundamental plane and is rotated 90 deg in the direction of motion on the reference orbit, and the $\hat{\boldsymbol{z}}$ axis completes the setup to yield a Cartesian dextral system.

The configuration space for the relative spacecraft dynamics in $\mathcal{L}$ is $\mathbb{R}^3$. Let $T_S(\mathbb{R}^3) = \mathbb{R}^3 \times \mathbb{R}^3$ be the tangent space of $\mathbb{R}^3$. Given a spacecraft S_i: $i \in \{1, \ldots, N\}$, we use $(\boldsymbol{\rho}_i, \dot{\boldsymbol{\rho}}_i)$ as coordinates for $T_S(\mathbb{R}^3)$, viz., $(\boldsymbol{\rho}_i, \dot{\boldsymbol{\rho}}_i) \in T_S(\mathbb{R}^3)$, $\boldsymbol{\rho}_i = [x_i, y_i, z_i]^T$ and $\dot{\boldsymbol{\rho}}_i = [\dot{x}_i, \dot{y}_i, \dot{z}_i]^T$. The differential equations of the dynamics of S_i in the rotating frame $\mathcal{L}$ can be written in the state-space form (cf. [5,6])

$$\frac{\mathrm{d}}{\mathrm{d}t}\begin{bmatrix}\boldsymbol{\rho}_i\\ \dot{\boldsymbol{\rho}}_i\end{bmatrix} = \begin{bmatrix}0_{3\times3} & I_3\\ A_r & A_{\dot{r}}\end{bmatrix}\begin{bmatrix}\boldsymbol{\rho}_i\\ \dot{\boldsymbol{\rho}}_i\end{bmatrix} + \begin{bmatrix}0_{3\times3}\\ I_3\end{bmatrix}\left(-\frac{\mu(\boldsymbol{\rho}_i+\boldsymbol{R})}{||\boldsymbol{\rho}_i+\boldsymbol{R}||^3} + \frac{\mu}{a_{\mathrm{ref}}^2}\hat{\boldsymbol{x}} + \boldsymbol{f}_i\right) \tag{6}$$

where $\boldsymbol{\rho}_i(0) = \boldsymbol{\rho}_{i0}$, $\dot{\boldsymbol{\rho}}_i(0) = \dot{\boldsymbol{\rho}}_{i0}$,

$$A_r = \begin{bmatrix}n_{\mathrm{ref}}^2 & 0 & 0\\ 0 & n_{\mathrm{ref}}^2 & 0\\ 0 & 0 & 0\end{bmatrix}, \qquad A_{\dot{r}} = \begin{bmatrix}0 & 2n_{\mathrm{ref}} & 0\\ -2n_{\mathrm{ref}} & 0 & 0\\ 0 & 0 & 0\end{bmatrix} \tag{7}$$

$\boldsymbol{R} \triangleq [a_{\mathrm{ref}}, 0, 0]^T$, a_{ref} is the radius of the reference orbit, and μ is the gravitational constant. $\boldsymbol{f}_i \in \mathbb{R}^3$ is the specific force control vector applied by the ith spacecraft, represented in frame $\mathcal{L}$.

We say that the spacecraft formation (or, alternatively, the formation graph F^N) is stable if the mean motion of S_i is commensurate with the mean motion of S_j (but not necessarily with n_{ref}) to form a 1:1 resonant motion, implying that the energy of S_i matches the energy of S_j (but not necessarily the energy of the reference orbit). This energy matching condition, which is necessary and sufficient to guarantee a stable formation, can be formulated simply as a semimajor axis matching [3]

$$a_i = a_j \tag{8}$$

or, in terms of the position and velocity component in $\mathcal{L}$, as $\varepsilon_i = \varepsilon_j$, where the total energy ε_i is given by

$$\varepsilon_i = \frac{1}{2}\{(\dot{x}_i - n_{\mathrm{ref}}y_i)^2 + [\dot{y}_i + n_{\mathrm{ref}}(x_i + a_{\mathrm{ref}})]^2 + \dot{z}_i^2\} - \frac{\mu}{\sqrt{(a_{\mathrm{ref}}+x_i)^2 + y_i^2 + z_i^2}} \tag{9}$$

Approximate solutions for the configuration space of the formation, used in the sequel, can be obtained by linearization of Eq. (6) about the origin, taking $\|\boldsymbol{\rho}_i\|/a_{\mathrm{ref}}$ to be first order small. The resulting well-known Clohessy–Wiltshire (CW) equations [17] for relative orbital motion are

$$\frac{\mathrm{d}}{\mathrm{d}t}\begin{bmatrix}\Delta\boldsymbol{\rho}_i\\ \Delta\dot{\boldsymbol{\rho}}_i\end{bmatrix} = \begin{bmatrix}0_{3\times3} & I_3\\ (A_r)_{\mathrm{lin}} & (A_{\dot{r}})_{\mathrm{lin}}\end{bmatrix}\begin{bmatrix}\Delta\boldsymbol{\rho}_i\\ \Delta\dot{\boldsymbol{\rho}}_i\end{bmatrix} + \begin{bmatrix}0\\ I_3\end{bmatrix}\Delta\boldsymbol{f}_i \tag{10}$$

where

$$(A_r)_{\mathrm{lin}} = \begin{bmatrix}3n_{\mathrm{ref}}^2 & 0 & 0\\ 0 & 0 & 0\\ 0 & 0 & -n_{\mathrm{ref}}^2\end{bmatrix}, \qquad (A_{\dot{r}})_{\mathrm{lin}} = \begin{bmatrix}0 & 2n_{\mathrm{ref}} & 0\\ -2n_{\mathrm{ref}} & 0 & 0\\ 0 & 0 & 0\end{bmatrix} \tag{11}$$

and $\Delta\boldsymbol{f}_i \in \mathbb{R}^3$ is the linearized control vector.

In this work, we use the nonlinear dynamical model (6) to investigate the following control problem: Suppose that there exists a sensor which provides LOS measurements only. Each spacecraft S_i then tracks its neighboring spacecraft, S_{i+1}, and the last spacecraft, S_N, tracks S_1, to form the Hamiltonian cycle C^N (cf. Fig. 1) whose edges are the directed measurement vectors. Is there a LOS-feedback control law that renders C^N a stable formation in the sense of Eq. (8)?

IV. Cyclic Formation Control Laws

The proposed continuous-thrust feedback controller is designed based on LOS bearing and range measurements only. Such measurements can be acquired by several methods, such as the use of vision-based sensors that combine star trackers and optical/RF ranging [10], or a combination of onboard optical tracking with rate gyros for the determination of the inertial LOS. In any case, only the relative LOS vector is required for the control; there is no need for the measurement of the absolute position of each satellite (e.g., GPS position measurements are unavailable). This LOS-based control of the cyclic formation $F^N \equiv C^N$ couples the dynamics of all spacecraft. In this section, we shall assume that C^N is a Hamiltonian cycle, that is, includes all the FF spacecraft. We shall discuss regular cycles, $C^m \subset F^N$, $m < N$, in Sec. V.

In a typical formation flying setting, the spacecraft initially have different SMAs, hence the uncontrolled motion will result in a relative drift, and eventually the formation will break apart. The objective of the controller is to eliminate the secular relative position drift among the spacecraft, or, in other words, to establish energy matching among the spacecraft orbits (but not necessarily relative to the reference orbit). This will stop the drift, but the formation may spread during the uncontrolled preestablishment phase and may require a separate reconfiguration maneuver.

In the sequel, we distinguish between two cases. The first is the use of a full controller, where both LOS range and bearing are measured, and a reduced controller, where only the LOS bearing is measured. The following sections develop control laws for both cases.

A. Control Using LOS Bearing and Range

Suppose that $S_i \in C^N$ tracks $S_j \in C^N$, as shown in Fig. 1. The LOS vector at time t, $\ell_i(t)$, is defined by

$$\ell_i(t) = \boldsymbol{\rho}_j(t) - \boldsymbol{\rho}_i(t) \tag{12}$$

where, for $N \geq 3$,

$$j = \begin{cases} i+1 & 1 \leq i < N \\ 1 & i = N \end{cases} \tag{13}$$

If S_i and S_j have the same orbital period, then $\ell_i(t)$ is identical (in magnitude and direction) to the LOS vector $\ell_i(t-T)$, where T is the orbital period of the reference orbit. On the other hand, a mismatch of the orbital periods will result in secular angular and magnitude error between the instantaneous inertial LOS vectors at times t and $t-T$.

To correct for these orbital periods/energy mismatch, the difference $\ell_i(t) - \ell_i(t-T)$ is used as feedback, generating a control force that equalizes the orbital periods. The resulting control law may therefore be formulated as

$$\boldsymbol{f}_i = \begin{cases} 0 & t \leq T \\ -K_i[\ell_i(t) - \ell_i(t-T)] & t > T \end{cases} \tag{14}$$

where K_i is the scalar feedback gain.

A natural question is whether the proposed controller (14) is stable. Keeping in mind that the objective of the control law (14) is to match the orbital periods of the spacecraft, suppose that there exists a steady-state common SMA $\forall\ S_i \in C^N$, denoted by a_{eq}, which is not necessarily equal to a_{ref}. The SMA of some $S_i \in C^N$ can be therefore written as

$$a_i = a_{\text{ref}} + \Delta a_i \tag{15}$$

Stability is determined by studying the closed-loop dynamics of the SMAs of the formation. Conforming with the stability definition (8), a stabilizing controller is defined as a control law for which $\lim_{t\to\infty} a_i(t) = \lim_{t\to\infty} a_j(t)$, or, in other words,

$$\lim_{t\to\infty} \Delta a_i(t) = \lim_{t\to\infty} \Delta a_j(t) = \Delta a_{\text{ss}} = \text{const} \tag{16}$$

for arbitrary initial conditions $\Delta a_i(0)$, $\Delta a_j(0)$.

To study the dynamics of the SMA, we use Gauss's variational equation for the SMA for some $S_i \in C^N$, given by (cf. [18], p. 489)

$$\dot{a}_i = \frac{2a_i^2}{\mu} V_i f_{t_i} \tag{17}$$

Here f_{t_i} is the tangential component of the control force along the velocity vector $\boldsymbol{V}_i$, that is, $f_{t_i} = \boldsymbol{f}_i \cdot \hat{\boldsymbol{V}}_i$, and $V_i = \|\boldsymbol{V}_i\|$. The control force vector $\boldsymbol{f}_i$ is given by Eq. (14).

We can now perform a linear stability analysis for nearly circular orbits. Letting e_i be the eccentricity of S_i's orbit , we may use the vis-viva equation to write

$$V_i = \sqrt{\frac{\mu}{a_i}}[1 + \mathcal{O}(e_i)] \tag{18}$$

Substituting Eqs. (15) and (18) into Eq. (17) yields

$$\dot{a}_i = \Delta\dot{a}_i = \frac{2}{\sqrt{\mu}} a_{\text{ref}}^{3/2}\left(1 + \frac{\Delta a_i}{a_{\text{ref}}}\right)^{3/2}[1 + \mathcal{O}(e_i)] f_{t_i} \tag{19}$$

where, by keeping only first-order terms in Δa_i and e_i, we obtain the linear variational equation

$$\Delta\dot{a}_i = \frac{2}{n_{\text{ref}}} \Delta f_{t_i} \tag{20}$$

where $n_{\text{ref}} = \sqrt{\mu/a_{\text{ref}}^3}$ is the mean motion of the equilibrium orbit.

We now observe that for nearly circular orbits, the tangential component and the $\hat{\boldsymbol{y}}$ component of the control acceleration are approximately equal,

$$f_{t_i} = \boldsymbol{f}_i \cdot \hat{\boldsymbol{V}} \approx \boldsymbol{f}_i \cdot \hat{\boldsymbol{y}} \tag{21}$$

Next, we linearize the expression for the control force, given in Eq. (14), and assume for simplicity that $K_i = K\ \ \forall\ i$. The instantaneous LOS at time t is given by

$$\ell_i(t, a_j, a_i) = \boldsymbol{\rho}_j(t, a_j) - \boldsymbol{\rho}_i(t, a_i) \tag{22}$$

Linearizing about a_{ref} entails the relationship

$$\ell_i(t, a_j, a_i) = \boldsymbol{\rho}_j(t, a_{\text{ref}}) + \frac{\partial \boldsymbol{\rho}_j(t, a_{\text{ref}})}{\partial a}\Delta a_j - \left[\boldsymbol{\rho}_i(t, a_{\text{ref}}) + \frac{\partial \boldsymbol{\rho}_i(t, a_{\text{ref}})}{\partial a}\Delta a_i\right] \tag{23}$$

Similarly, the LOS at time $t - T$, up to higher-order terms, is given by

$$\ell_i(t-T, a_j, a_i) = \boldsymbol{\rho}_j(t-T, a_{\text{ref}}) + \frac{\partial \boldsymbol{\rho}_j(t-T, a_{\text{ref}})}{\partial a}\Delta a_j - \left[\boldsymbol{\rho}_i(t-T, a_{\text{ref}}) + \frac{\partial \boldsymbol{\rho}_i(t-T, a_{\text{ref}})}{\partial a}\Delta a_i\right] \tag{24}$$

All the partial derivatives are calculated at the reference orbit. Substituting into the control law (14) and taking the first-order terms only gives

$$\mathbf{f}_i = -K\Bigg[\boldsymbol{\rho}_j(t, a_{\text{ref}}) - \boldsymbol{\rho}_j(t-T, a_{\text{ref}}) - [\boldsymbol{\rho}_i(t, a_{\text{ref}}) - \boldsymbol{\rho}_i(t-T, a_{\text{ref}})] + \left(\frac{\partial \boldsymbol{\rho}_j(t, a_{\text{ref}})}{\partial a} - \frac{\partial \boldsymbol{\rho}_j(t-T, a_{\text{ref}})}{\partial a}\right)\Delta a_j - \left(\frac{\partial \boldsymbol{\rho}_i(t, a_{\text{ref}})}{\partial a} - \frac{\partial \boldsymbol{\rho}_i(t-T, a_{\text{ref}})}{\partial a}\right)\Delta a_i\Bigg] \tag{25}$$

The first four terms in the brackets of Eq. (25) form a steady-state periodic control force, $\boldsymbol{f}_{\text{ss}i}$. Therefore, we may rewrite Eq. (25) as follows:

$$\boldsymbol{f}_i = \boldsymbol{f}_{\text{ss}i} - K\left(\frac{\partial \boldsymbol{\rho}_j(t, a_{\text{ref}})}{\partial a} - \frac{\partial \boldsymbol{\rho}_j(t-T, a_{\text{ref}})}{\partial a}\right)\Delta a_j + K\left(\frac{\partial \boldsymbol{\rho}_i(t, a_{\text{ref}})}{\partial a} - \frac{\partial \boldsymbol{\rho}_i(t-T, a_{\text{ref}})}{\partial a}\right)\Delta a_i \tag{26}$$

where $\boldsymbol{f}_{\text{ss}i} = -K[\ell_i(t, a_{\text{ref}}) - \ell_i(t-T, a_{\text{ref}})]$ is the steady-state control force.

The $\hat{\boldsymbol{y}}$ component of this force is now substituted into the linearized variational equation (20). Expanding and keeping only first-order terms with Δa, we obtain

$$\Delta\dot{a}_i = \frac{2}{n_{\text{ref}}}\left[f_{\text{ss}yi} - K\left(\frac{\partial y_j(t, a_{\text{ref}})}{\partial a} - \frac{\partial y_j(t-T, a_{\text{ref}})}{\partial a}\right)\Delta a_j + K\left(\frac{\partial y_i(t, a_{\text{ref}})}{\partial a} - \frac{\partial y_i(t-T, a_{\text{ref}})}{\partial a}\right)\Delta a_i\right] \tag{27}$$

Here $f_{\text{ss}yi} = \boldsymbol{f}_{\text{ss}i} \cdot \hat{\boldsymbol{y}}$ is the y component of $\boldsymbol{f}_{\text{ss}i}$.

Equation (27) describes the dynamics of the SMA of S_i. It is a linear time-varying differential equation. The coefficients of Eq. (27) map the dynamics of the orbital coordinates of the satellite in frame $\mathcal{L}$ into the orbital elements space. Here we are interested in establishing the closed-loop stability of Δa, which is a slowly varying quantity. Therefore we can perform a time-scale separation by averaging Eq. (27) over one orbital period, thus isolating the slow dynamics of Δa.

Starting with averaging the steady-state constituent, we note that because the values of the LOS vector are calculated at the reference, all of the satellites must have the same SMA. Hence the integral of the LOS difference over one orbital period is identically zero:

$$\int_{t-T}^{t} \boldsymbol{f}_{\text{ss}i} \cdot \hat{\boldsymbol{y}}\, \mathrm{d}t = -K\int_{t-T}^{t} [\ell_i(t, a_{\text{ref}}) - \ell_i(t-T, a_{\text{ref}})] \cdot \hat{\boldsymbol{y}}\, \mathrm{d}t \equiv 0 \tag{28}$$

When averaging the remaining terms, we obtain the same average for all spacecraft:

$$\frac{1}{T}\int_{t-T}^{t}\left(\frac{\partial y_i(t, a_{\text{ref}})}{\partial a} - \frac{\partial y_i(t-T, a_{\text{ref}})}{\partial a}\right)\mathrm{d}t = \frac{1}{T}\int_{t-T}^{t}\left(\frac{\partial y_j(t, a_{\text{ref}})}{\partial a} - \frac{\partial y_j(t-T, a_{\text{ref}})}{\partial a}\right)\mathrm{d}t \equiv D \tag{29}$$

As shown in Appendix A, $y(t) < y(t-T)$ when a increases, and therefore $D < 0$. Consequently, the closed-loop Δa dynamics for some $S_i \in C^N$ can be written as

$$\Delta\dot{a}_i = -\frac{2}{n_{\text{ref}}} KD[\Delta a_j - \Delta a_i] \tag{30}$$

and the overall closed-loop dynamics for C^N becomes

$$\begin{bmatrix} \Delta\dot{a}_1 \\ \Delta\dot{a}_2 \\ \vdots \\ \Delta\dot{a}_N \end{bmatrix} = -\frac{2}{n_{\text{ref}}} KD \begin{bmatrix} -1 & 1 & 0\cdots & 0 \\ 0 & -1 & 1\cdots & 0 \\ \cdots & \cdots & \cdots & \cdots \\ 1 & 0 & 0\cdots & -1 \end{bmatrix} \begin{bmatrix} \Delta a_1 \\ \Delta a_2 \\ \vdots \\ \Delta a_N \end{bmatrix} \tag{31}$$

If we let $k = -2KD/n_{\text{ref}}$, $\Delta\boldsymbol{a} = [\Delta a_1, \Delta a_1, \ldots, \Delta a_N]^T$ and $A = \text{circ}(-k, k, 0, \ldots, 0)$, then Eq. (31) assumes the compact state-space form

$$\Delta\dot{\boldsymbol{a}} = A\Delta\boldsymbol{a} \tag{32}$$

The system matrix A is circulant with the generating row $[-k, k, 0, \ldots, 0]$ [cf. Eq. (1)]. Using Eqs. (4) and (5), the representer for this case is simply

$$p(\omega) = -k + k\omega \tag{33}$$

implying that the eigenvalues of the system matrix defining the state-space dynamics (31) are given by

$$\lambda_i = -k + k\omega^{i-1} = -k + ke^{2\pi I(i-1)/N}, \qquad i = 1, \ldots, N \tag{34}$$

Thus, one eigenvalue is zero, and the additional $N-1$ eigenvalues all have negative real parts provided that $k > 0$. Because $D < 0$, we conclude that system is stable for positive control gain, $K > 0$.

However, due to the presence of the zero eigenvalue, asymptotic stability, that is, $\lim_{t\to\infty}\Delta a_i(t) \to 0\ \forall\ i$, cannot be achieved. In fact, to achieve a bounded formation asymptotic stability is not required; based on the energy matching condition (8) it is sufficient that all steady-state SMAs are equal, implying that $\lim_{t\to\infty}\Delta a_i(t) \to \Delta a_{\text{ss}} = \text{const}\ \forall\ i$ [cf. Eq. (16)]. We shall now show that indeed all SMA differences converge to the same value, and moreover, that this value is the arithmetic mean of all the initial SMA differences, that is,

$$\Delta a_{\text{ss}} = \frac{1}{N}\sum_{i=1}^{N}\Delta a_i(0) \tag{35}$$

To that end, let us perform the transformation $\Delta\boldsymbol{a} = F\Delta\tilde{\boldsymbol{a}}$, where F is given by Eq. (2). The transformed state-space dynamics become

$$\Delta\dot{\tilde{\boldsymbol{a}}} = \Lambda\Delta\tilde{\boldsymbol{a}} \tag{36}$$

where Λ is a diagonal eigenvalue matrix with entries given by Eq. (34). The transition matrix of the transformed system (36) can be written as

$$e^{\Lambda t} = \text{diag}(1, e^{(-k+k\omega)t}, \ldots, e^{(-k+k\omega^{N-1})t}) \tag{37}$$

so that the steady-state values of the transformed states, $\Delta\tilde{\boldsymbol{a}}_{\text{ss}}$, can be calculated by taking the limit

$$\Delta\tilde{\boldsymbol{a}}_{\text{ss}} = \lim_{t\to\infty}(e^{\Lambda t})\Delta\tilde{\boldsymbol{a}}(0) = [\Delta\tilde{a}_1(0), 0, \ldots, 0]^T \tag{38}$$

Transforming back into the original system and noting that the first row (column) of the Hermitian matrix F is $[1, 1, \ldots, 1]$ [cf. Eq. (2)] yields

$$\begin{aligned}\Delta\boldsymbol{a}_{\text{ss}} &= F\lim_{t\to\infty}(e^{\Lambda t})F^* = \frac{1}{n}\cdot[1, 1, \ldots, 1]^T[1, 1, \ldots, 1]\Delta\boldsymbol{a}_0 \\ &= \frac{1}{N}\sum_{i=1}^{N}\Delta a_i(0)\cdot[1, 1, \ldots, 1]^T\end{aligned} \tag{39}$$

which provides the desired result.

B. Control Using LOS Bearing Only

We assume now that only the LOS bearing is measured, and that the interspacecraft range is unavailable. In this case only a unit vector in the direction of the LOS between S_i and S_j, denoted by $\hat{\boldsymbol{\ell}}_i$, is known (cf. Fig. 1):

$$\hat{\boldsymbol{\ell}}_i = \frac{\boldsymbol{\ell}_i}{\ell_i} = \frac{\boldsymbol{\rho}_j - \boldsymbol{\rho}_i}{\|\boldsymbol{\rho}_j - \boldsymbol{\rho}_i\|} \tag{40}$$

If the two spacecraft have the same orbital period, then the LOS unit vector at time t is parallel to the LOS unit vector at time $t - T$. A mismatch of the orbital periods results in an angular error between the LOS unit vectors.

Thus, the difference $\hat{\boldsymbol{\ell}}_i(t) - \hat{\boldsymbol{\ell}}_i(t-T)$ may be fed back to generate a control force acting on S_i in a direction perpendicular to both the LOS and the LOS rate. This control force acts to equalize the orbital periods. The reduced nonlinear control law is then

$$\boldsymbol{f}_i = \begin{cases} 0 & t \le T \\ -K_i[\hat{\boldsymbol{\ell}}_i(t) - \hat{\boldsymbol{\ell}}_i(t-T)] & t > T \end{cases} \tag{41}$$

The stability analysis of this controller is somewhat more involved than the stability analysis of the full controller and can be found in Appendix B, where it is shown that the stable closed-loop dynamics are

$$\Delta\dot{a}_i = -\frac{2}{n_{\text{ref}}} K_R D_R(\Delta a_j - \Delta a_i) \tag{42}$$

where $K_R > 0$, $D_R < 0$. Equation (42) has the same structure as the equation for the full controller, Eq. (30), and hence the graph-theoretic treatment of both cases is identical.

V. Leaders and Trees, Cycles and Tadpoles

A situation may arise in which S_i does not have a direct LOS to some S_j. This may result from a malfunction of the tracking system or from local geometric constraints. In this section, we shall investigate the dynamics of the formation in these cases. The treatment presented herein holds both for the full (LOS) and reduced (LOS bearing) controllers.

A. Leaders and Trees

A simple example for the inexistence of LOS due to geometric constraints is the case of linear formations, in which, instantaneously, all spacecraft form a line. In this case S_N cannot track S_1 since the LOS is blocked by the remaining $N-2$ spacecraft and the cycle breaks up to form a leader graph (i.e., a tree), as defined in Sec. II. Let us label the leader of this graph by S_N, with S_1 being the root. Per our definitions above, the spacecraft now form the leader formation L^N, that is $C^N \to L^N \equiv F^N$. This situation is shown in Fig. 2a.

Assuming a full LOS controller, the closed-loop dynamics (31) is transformed into

$$\begin{bmatrix} \Delta\dot{a}_1 \\ \Delta\dot{a}_2 \\ \vdots \\ \Delta\dot{a}_N \end{bmatrix} = k \begin{bmatrix} -1 & 1 & 0\cdots & 0 \\ 0 & -1 & 1\cdots & 0 \\ \cdots & \cdots & \cdots & \cdots \\ 0 & 0 & 0\cdots & 0 \end{bmatrix} \begin{bmatrix} \Delta a_1 \\ \Delta a_2 \\ \vdots \\ \Delta a_N \end{bmatrix} \tag{43}$$

where $k = -2KD/n_{\text{ref}}$ for the full controller and $k = -2K_1D_1/n_{\text{ref}}$ for the reduced controller. The system matrix of Eq. (43) is upper diagonal with $N-1$ eigenvalues equal to $-k$ and a single eigenvalue located at the origin. A solution of Eq. (43), taking advantage of the upper diagonal structure, can be written for each state variable, Δa_i, as follows:

$$\Delta a_i(t) = \begin{cases} \Delta a_N(0) + \sum_{m=0}^{N-i-1}\frac{(tk)^m}{m!}e^{-tk}[\Delta a_{i+m}(0) - \Delta a_N(0)], & i < N \\ \Delta a_N(0), & i = N \end{cases} \tag{44}$$

Therefore, at steady state,

$$\lim_{t\to\infty}\Delta a_i(t) = \Delta a_N(0), \qquad i = 1, \ldots, N \tag{45}$$

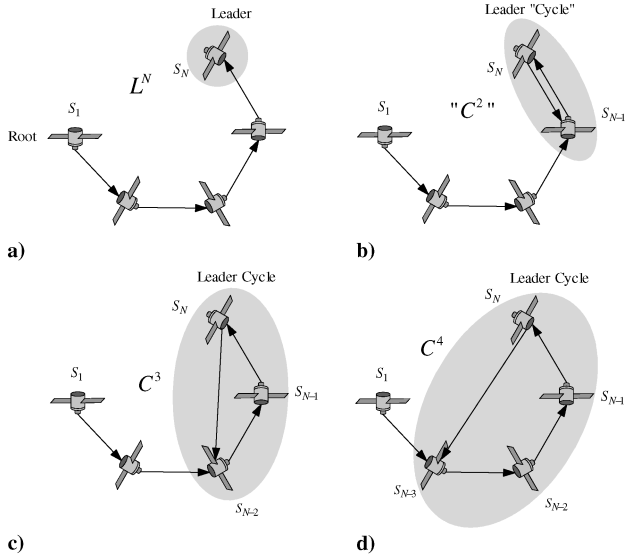

Fig. 2 a) Leader formation formed due to tracking loss renders a tree; b) degenerate leader cycle; leader cycle of c) three and d) four spacecraft forming a tadpole formation.

In other words, in a formation of the form L^N, the LOS controllers still render the formation stable in the sense of Eq. (8), albeit the SMAs of all the spacecraft in the formation tend toward the (uncontrolled) SMA of the leader. This is fundamentally different from the cyclic formation, in which the LOS controller steered the spacecraft onto an average SMA which was the centroid of the initial SMAs of all spacecraft. Thus, if the leader spacecraft accumulates an SMA error Δa_N, the L^N topology will force the follower spacecraft to form commensurate motion by modifying (increasing or decreasing) the follower spacecraft SMAs to that of the leader. In the C^N topology, the initialization errors $\Delta a_i(0)$ are averaged among all formation members. In this sense, we conclude that the C^N formation is more robust to initialization errors, as it is inherently leader independent.

B. Cycles and Tadpoles

Assume that after the Hamiltonian cycle breakup and the transformation into the leader formation, $C^N \to L^N$, the leader S_N regains tracking of some S_j, $j = 2, \ldots, N-1$. For $1 < j < N-1$, the formation graph contains the cycle C^{N-j+1}, as illustrated by Figs. 2c and 2d for the cases C^3 and C^4, respectively. The case $j = 1$ corresponds to the Hamiltonian cycle studied in Sec. IV and will be excluded from the current discussion. The case $j = N-1$ forms a degenerate cycle, as shown in Fig. 2b, and is denoted by C^2. We shall call the cycle C^{N-j+1}, $1 < j \leq N-1$, a leader cycle.

The closed-loop linearized dynamics of the formation graph, $F^N \supset C^{N-j+1}$, can be written as

$$\Delta\dot{\boldsymbol{a}} = \bar{A}\Delta\boldsymbol{a} \tag{46}$$

where $\bar{A}$ is the upper block-triangular matrix

$$\bar{A} = \begin{bmatrix} A_{11} & A_{12} \\ 0 & A_{22} \end{bmatrix} \tag{47}$$

In Eq. (47), A_{11} is an upper triangular $(j-1)\times(j-1)$ Toeplitz matrix of the form

$$A_{11} = \begin{bmatrix} -k & k & 0 & \cdots & 0 \\ 0 & -k & k & 0 & \vdots \\ \vdots & \ddots & \ddots & \ddots & 0 \\ 0 & 0 & 0 & -k & k \end{bmatrix} \tag{48}$$

and $A_{22} = \mathrm{circ}[-k, k, 0, \ldots, 0]$ is an $(N-j+1)\times(N-j+1)$ circulant matrix. It is obvious that the eigenvalues of $\bar{A}$ are those of A_{11} and A_{22}, that is,

$$\lambda_i(\bar{A}) = \begin{cases} \lambda_i(A_{11}) = -k, & i = 1, \ldots, j-1 \\ \lambda_i(A_{22}) = -k + ke^{2\pi I(i-j)/(N-j+1)}, & i = j, \ldots, N \end{cases} \tag{49}$$

Thus, the dynamics (46) are stable in the sense of Eq. (8); it contains $N-1$ eigenvalues with negative real parts and a single eigenvalue at the origin (obtained when $i = j+1$).

Let $\boldsymbol{w} = [w_1, w_2, \ldots, w_n]$ be the eigenvector associated to the zero eigenvalue; then $\boldsymbol{w} \in \mathrm{Null}(\bar{A})$ and $\bar{A}\boldsymbol{w} = \boldsymbol{0}$, which, upon substitution into Eqs. (47) and (48) implies that all the components of $\boldsymbol{w}$ are equal, that is, $w_1 = w_2 = \cdots = w_n$. Thus, at steady state all the components of $\Delta\boldsymbol{a}$ must be equal as well,

$$\Delta a_{\mathrm{ss}1} = \Delta a_{\mathrm{ss}2} = \ldots \Delta a_{\mathrm{ss}N} = \Delta a_{\mathrm{ss}} = \mathrm{const} \tag{50}$$

To determine Δa_{ss}, we note that the state transition matrix of Eq. (46) can be written as

$$\Phi(t) = \begin{bmatrix} e^{A_{11}t} & \Phi_{12}(t) \\ 0 & e^{A_{22}} \end{bmatrix} \tag{51}$$

Using Eq. (49), defining the eigenvalues, and using the observation (35), namely, that a circulant system matrix yields a steady-state value which is the centroid of all the initial state variables, we can evaluate the steady-state value of $\Phi(t)$:

$$\begin{aligned} \Delta\boldsymbol{a}_{\mathrm{ss}} &= \lim_{t\to\infty}\Phi(t) = \Phi(t) \\ &= \begin{bmatrix} 0 & C_{12} \\ 0 & C_{22} \end{bmatrix}\begin{bmatrix} \Delta\boldsymbol{a}_1(0) \\ \Delta\boldsymbol{a}_2(0) \end{bmatrix} = \begin{bmatrix} C_{12}\Delta\boldsymbol{a}_2(0) \\ C_{22}\Delta\boldsymbol{a}_2(0) \end{bmatrix} \end{aligned} \tag{52}$$

where C_{22} is an $(N-j+1)\times(N-j+1)$ matrix with entries equal to $1/(N-j+1)$ [cf. Eq. (39)]. However, based on Eq. (50), we must have $C_{12} = C_{22}$ and hence the sought for steady-state value of the SMA deviations from the reference value is given by

$$\Delta a_{\mathrm{ss}} = \frac{1}{N-j+1}\sum_{i=1}^{N-j+1}\Delta a_i(0) \tag{53}$$

Equation (53) establishes a remarkable fact: The semimajor axes of all formation members will converge to the average of the semimajor axes of those spacecraft forming a cycle.

This observation sheds light on the terminology leader cycle introduced previously: The initial SMAs of the spacecraft forming a cycle determine the steady-state behavior of all the formation. The case of a Hamiltonian cycle and the leader formation are thus both special cases of the leader cycle formation: in the Hamiltonian cycle cases, all spacecraft are equal "leaders" in the sense of determining the steady-state behavior of the formation; and in the single-leader formation only the leader determines the steady-state behavior of the formation. For example, referring to Fig. 2b, the steady-state value of the SMA will be $\Delta a_{\mathrm{ss}} = [\Delta a_N(0) + \Delta a_{N-1}(0)]/2$; in the case of Fig. 2c $\Delta a_{\mathrm{ss}} = [\Delta a_N(0) + \Delta a_{N-1}(0) + \Delta a_{N-2}(0)]/3$, and so on. Referring to the graphics of Fig. 2, it is convenient to think as if the leader cycle "drags" the tail of remaining spacecraft. Using a zoological analogy, it is tempting to describe the resulting structure as a tadpole formation.

VI. Illustrating Example

To illustrate the performance of the LOS-based controllers developed herein, we have carried out a simulation study. Dynamical simulations of the controlled and uncontrolled motions were performed for formations of three spacecraft. We emphasize that in all the simulations, the full, nonlinear model of Eq. (6) was used.

For illustration, we consider the case of a circular formation. The required initial conditions for forming a circular formation in the Euler–Hill frame (using the linear model for generating initial conditions only) are given by

Table 1 Initial conditions

S/C	x_0/a_{ref}	y_0/a_{ref}	z_0/a_{ref}	$\dot{x}_0/(n_{\text{ref}}a_{\text{ref}})$	$\dot{y}_0/(n_{\text{ref}}a_{\text{ref}})$	$\dot{z}_0/(n_{\text{ref}}a_{\text{ref}})$
No. 1	0.00005	0	0.0000866	0	−0.000101	0
No. 2	−0.000025	−0.0000866	−0.0000433	−0.0000433	0.0000505	−0.000075
No. 3	−0.000025	0.0000866	−0.0000433	0.0000433	0.00005	0.000075

$$\dot{y}_0 = -2nx_0, \qquad \dot{x}_0 = ny_0/2, \qquad z_0 = \sqrt{3}x_0, \qquad \dot{z}_0 = \sqrt{3}\dot{x}_0 \tag{54}$$

The actual initial conditions in our test scenario included slight violations of Eq. (54), so that each spacecraft had a slightly different SMA. As a result, the uncontrolled motion drifts apart. The numerical values of the initial conditions are summarized in Table 1.

The results of the open-loop simulation are depicted by Fig. 3. Figure 3a shows the normalized uncontrolled orbit projection on the xy plane. As expected, spacecraft (S/C) no. 1 and no. 2 drift away. The normalized distance, d/a_{ref}, between each spacecraft pair increases, as shown in Fig. 3b.

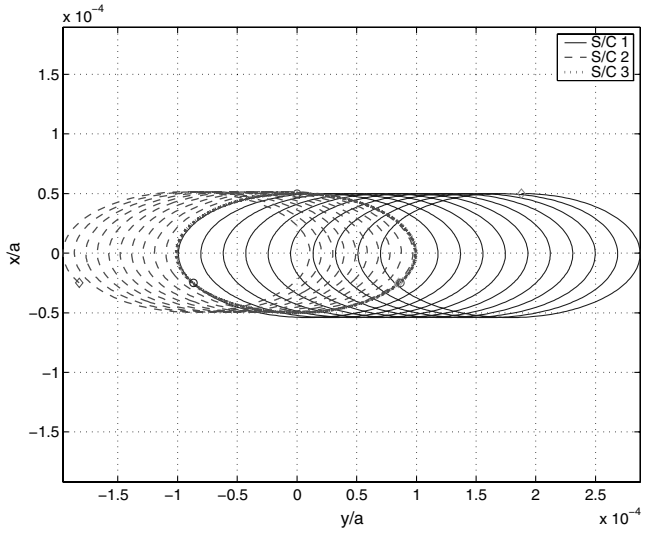

a)

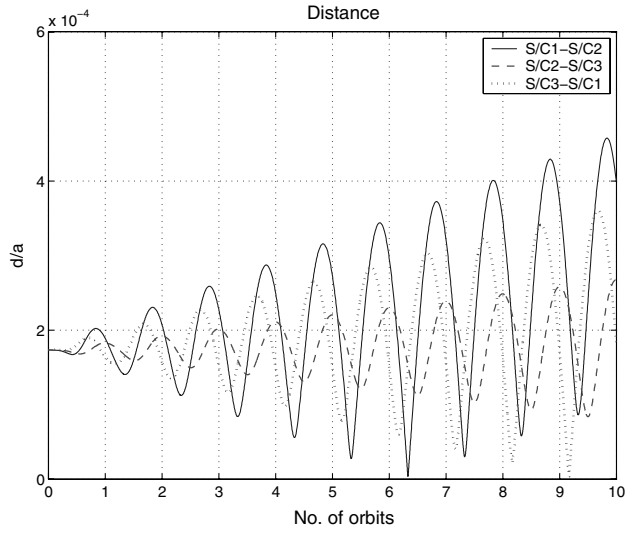

b)

Fig. 3 Uncontrolled motion: a) projection on the xy plane and b) distance between spacecraft.

A. Full Controller

In the closed-loop case with the full feedback LOS controller, the LOS error between two consecutive orbits is used as feedback [cf. Eq. (14)]. Figure 4a depicts the (normalized) projection of the controlled motion on the xy plane relative to the reference orbit. Comparing to the uncontrolled motion, it can be seen that in the controlled case all the spacecraft approach the same steady-state drift rate with respect to the original reference point. The relative drift is then stopped, as shown in Fig. 4b. In this simulation, we used the feedback gain $K = 3 \times 10^{-3}$.

The distance between each satellite pair is shown in Fig. 5. Comparing to the uncontrolled motion (Fig. 3b), we see that the drift stops and the distance is bounded, as expected. The normalized components of the control accelerations are shown in Fig. 6. It is seen

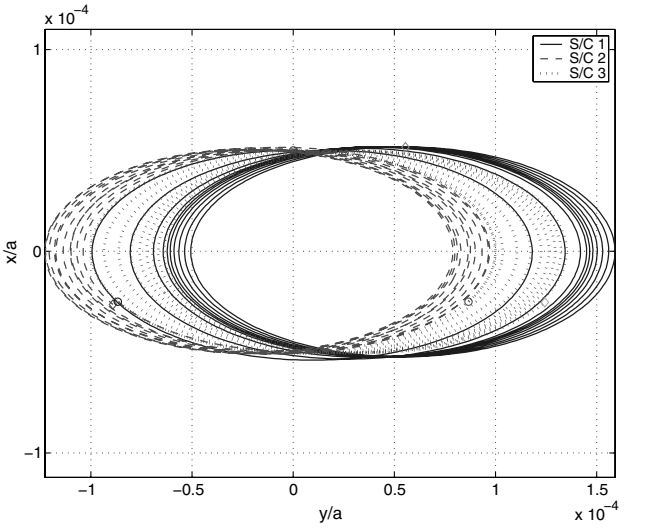

a)

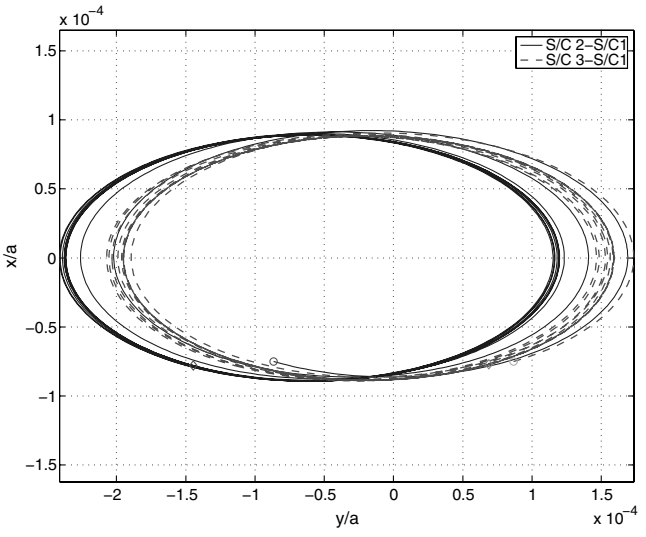

b)

Fig. 4 Controlled motion, full controller: a) xy projection shows drift relative to reference orbit and b) xy projection relative to S/C no. 1 shows bounded relative motion.

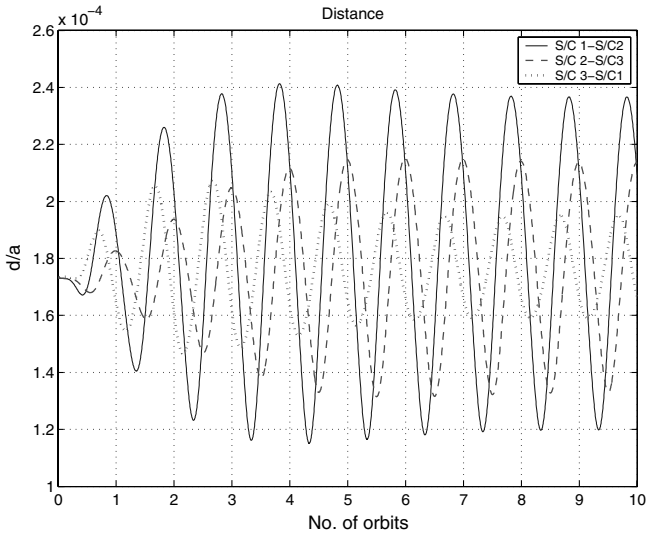

Fig. 5 The full controller maintains a bounded relative distance between each pair of spacecraft.

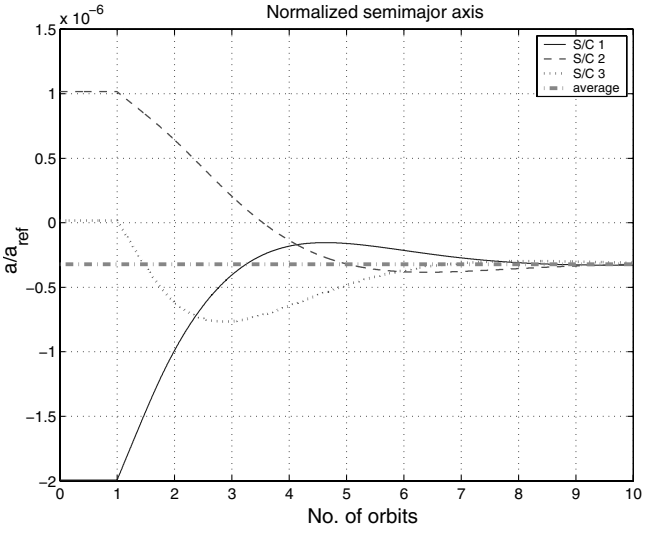

Fig. 7 Instantaneous semimajor axes using the full controller converge to the average of the initial semimajor axes values.

that the most active component is the $\hat{y}$ component that acts to modify the SMA. Upon convergence, the control forces approach virtually zero values. The ΔV calculations for this controller are given in the sequel.

Next, we discuss the behavior of the instantaneous SMA of each satellite. The proposed control law acts to equalize the normalized initial SMA errors, as shown in Fig. 7. The SMAs of the spacecraft converge from the initial values to a common steady-state value, which equals the average of the initial SMAs. At this point, all of the spacecraft have equal drifts with respect to the reference frame, hence the formation stays together.

B. Reduced Controller

In this case, only the error of the LOS direction between two consecutive orbits is used as feedback. The controlled (normalized) distance between each satellite pair is shown in Fig. 8. The components of the control acceleration are shown in Fig. 9. The behavior of the instantaneous SMA is shown in Fig. 10. This simulation uses the feedback gain $K = 3 \times 10^{-7}$.

We now compare the performance of the reduced controller to the corresponding results for the uncontrolled motion and for the full controller. Both controllers arrest the relative position drift. The full controller, however, seems to perform better than the reduced controller. It converges faster; hence the steady-state dispersion of the formation is smaller. Comparing the behavior of the SMAs, we see that for the full controller the SMAs converge to the equilibrium value for the examined scenario. The reduced controller, however, yields slower convergence. The feedback gain should be chosen based on operational considerations. It is preferable to have the same gain for all spacecraft: choose a gain which yields adequate convergence rate and take into account the fuel and maximum acceleration limitations. The effect of gain on the convergence rate is illustrated in Fig. 11. In both cases, increasing the gain destabilizes the system. However, doubling the feedback gain in the reduced

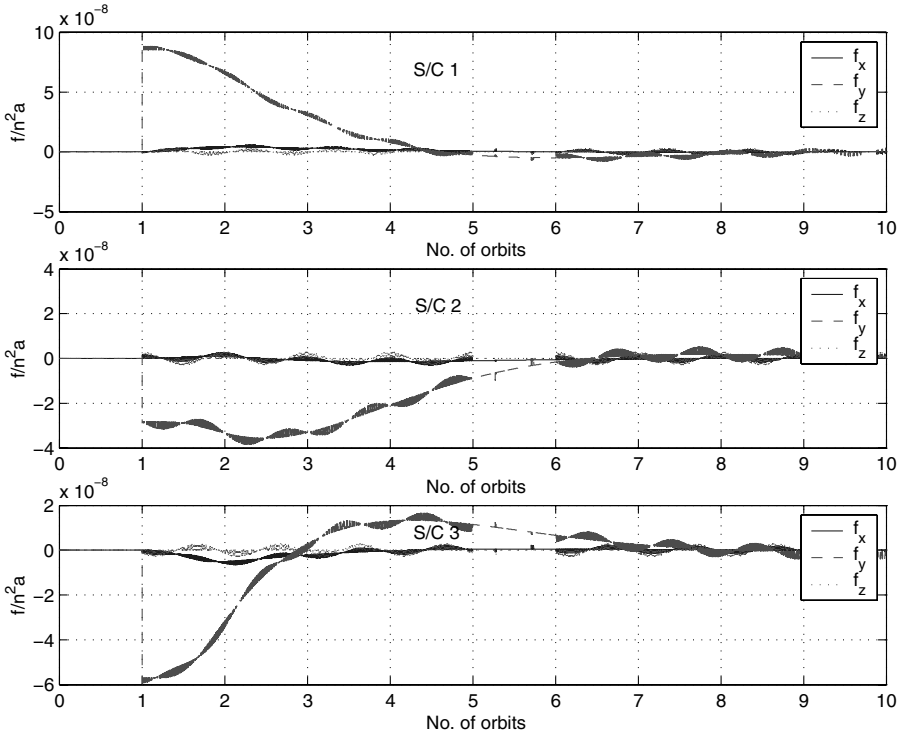

Fig. 6 Normalized control accelerations for the full controller.

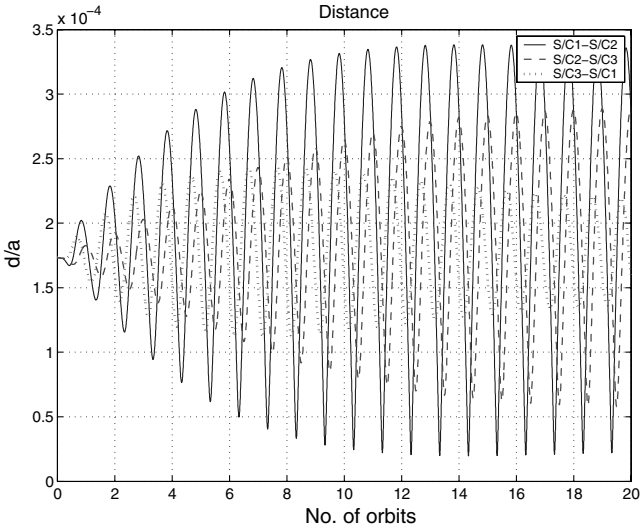

Fig. 8 The reduced controller maintains a bounded relative distance between each pair of spacecraft.

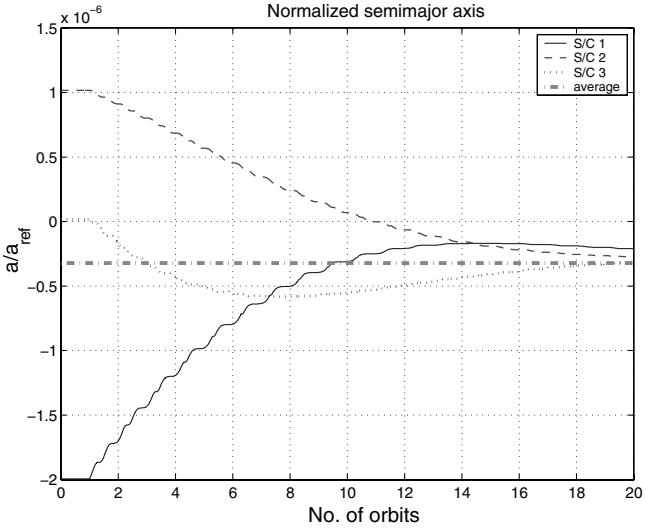

Fig. 10 Instantaneous semimajor axes using the reduced controller converge to the average of initial semimajor axes values.

controller case yields an improved time-domain behavior, and the SMAs converge faster to their steady-state values. ΔV calculations are discussed next.

C. Fuel Consumption

The fuel needed for the maneuver is related to the total velocity change, as calculated by integrating the magnitude of the control acceleration. The normalized velocity change is then

$$\frac{\Delta V_i}{(na)_{\text{ref}}} = \int_0^{t_f} [f_{x_i}^2 + f_{y_i}^2 + f_{z_i}^2]^{1/2} \frac{\mathrm{d}t}{(n^2 a)_{\text{ref}}}, \qquad i = 1 \cdots N \quad (55)$$

If the integration upper limit t_f exceeds the convergence time, then the resulting integral levels off and yields the total ΔV required for the maneuver for each spacecraft. The values of the normalized velocity change for our example are summarized in Table 2, for several combinations of control topologies and gain values. As a reference, we added the value of an equivalent impulsive velocity change that is required to change the semimajor axis of each spacecraft from the initial value to the equilibrium value. By taking the difference between the initial energy and the equilibrium energy and solving for $\Delta V_i = V_{\text{eq}_i} - V_{0_i}$, we obtain the impulsive velocity change needed for energy matching:

$$\left.\frac{\Delta V_i}{(na)_{\text{ref}}}\right|_{\text{IMPULSE}} = \sqrt{\left(\frac{V_{0_i}}{n_{\text{ref}} a_{\text{ref}}}\right)^2 - \left(\frac{1}{a_{\text{eq}}/a_{\text{ref}}} - \frac{1}{a_{0_i}/a_{\text{ref}}}\right)} - \frac{V_{0_i}}{n_{\text{ref}} a_{\text{ref}}}, \qquad i = 1 \cdots N \quad (56)$$

The choice of the adequate gain is therefore a tradeoff between the fuel consumption and the convergence time, subject to the available

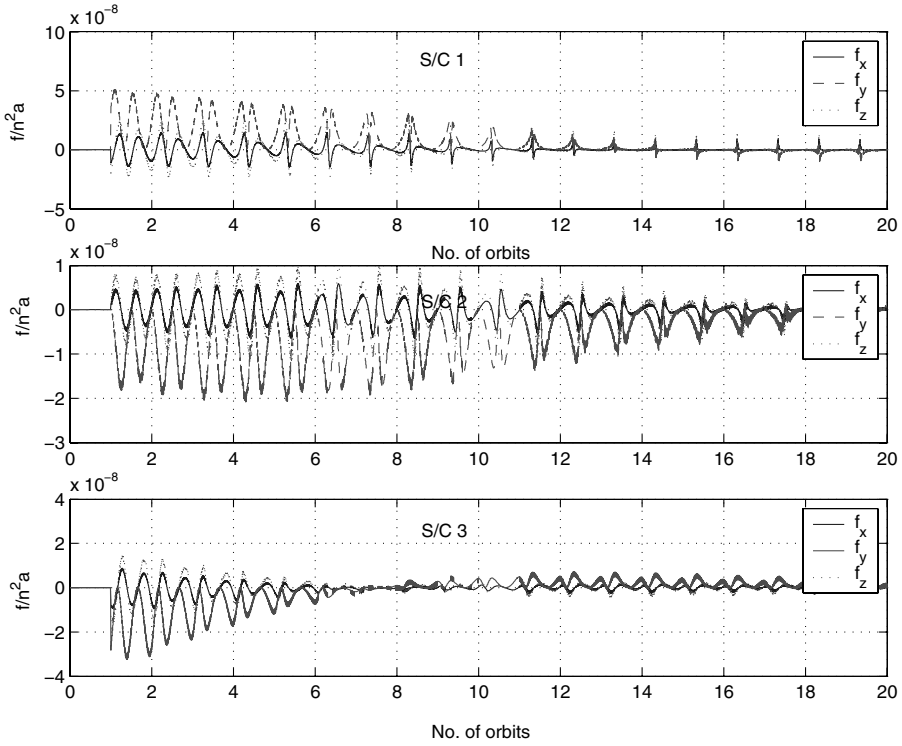

Fig. 9 Normalized control accelerations for the reduced controller.

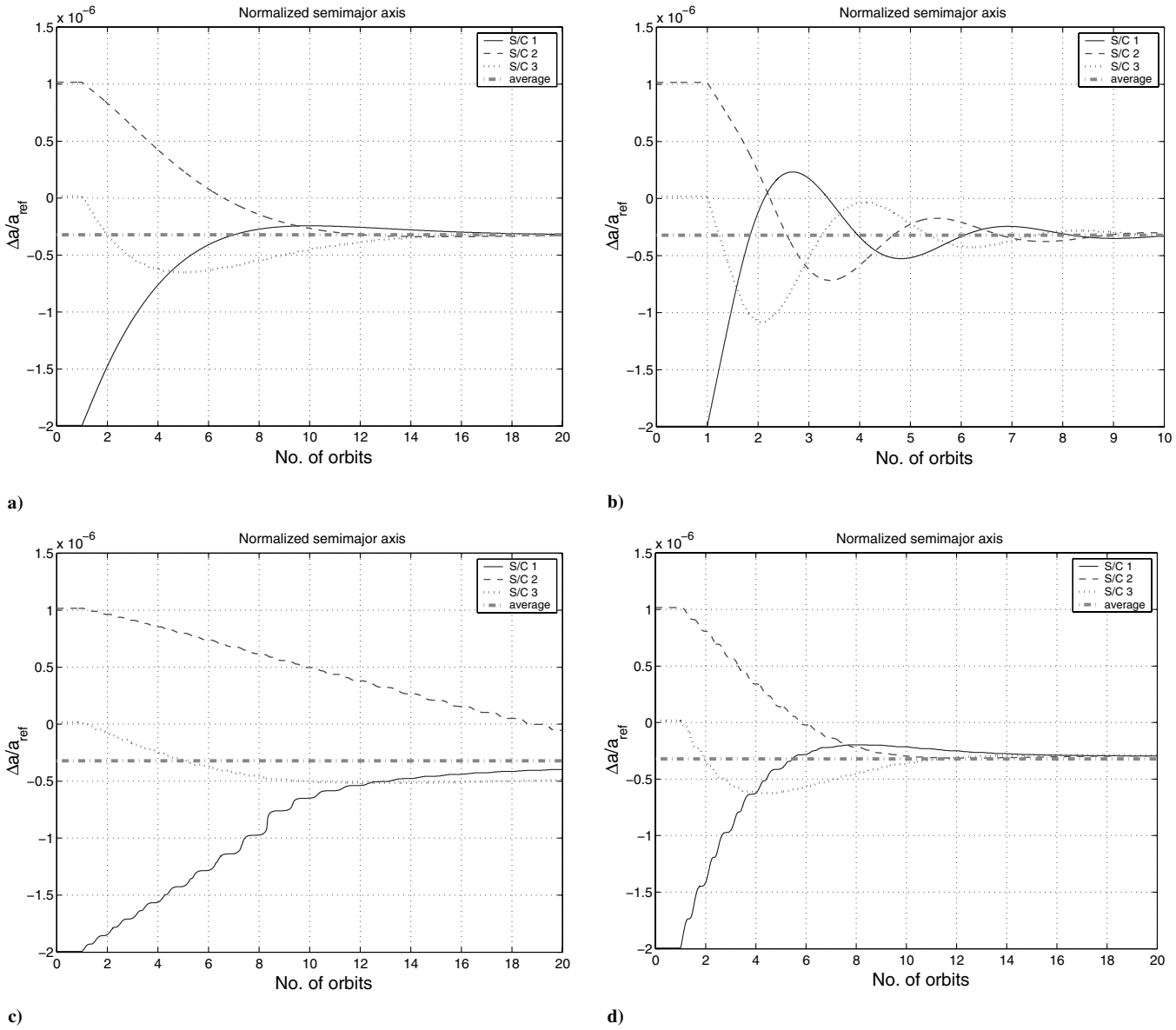

Fig. 11 Effect of feedback gain on the time history of the semimajor axis: a) full controller, $K = 1.5 \times 10^{-3}$ (half the nominal); b) full controller, $K = 6 \times 10^{-3}$ (twice the nominal); c) reduced controller, $K = 1.5 \times 10^{-7}$ (half the nominal); and d) reduced controller, $K = 6 \times 10^{-7}$ (twice the nominal).

maximum thrust. For example, suppose a 100 kg satellite in a low Earth orbit. The velocity change for S/C 1, using the full controller with the nominal gain, is about 8 mm/s. The maximum thrust (see Fig. 6) is about 10^{-4} N, which is a typical thrust of an electric propulsion system. To make the simulation more realistic, the effect of perturbations on the performance of the proposed control law was studied. The main perturbation that has a secular effect on the semimajor axis is the drag difference among the satellites.

D. Perturbations

Assuming that the formation is placed at an altitude of 500 km, and the nominal ballistic coefficient is 180 kg/m^2, the normalized drag acceleration is about 10^{-8}. Now suppose that there is a 10% difference between the drag accelerations of the satellites, that is, S/C 1 has normalized drag acceleration of 0.9×10^{-8}, S/C 2 has normalized drag acceleration of 1×10^{-8}, and S/C 3 has normalized drag acceleration of 1.1×10^{-8}. The behavior of the semimajor axes

Table 2 ΔV calculations

Controller	Gain	$\Delta V/(na)_{\text{ref}}$ S/C 1	S/C 2	S/C 3
Full	Nominal (0.003)	0.1013×10^{-5}	0.0732×10^{-5}	0.0639×10^{-5}
	Double (0.006)	0.1735×10^{-5}	0.1304×10^{-5}	0.1413×10^{-5}
	Half (0.0015)	0.08998×10^{-5}	0.06779×10^{-5}	0.04928×10^{-5}
Reduced	Nominal (3×10^{-7})	0.1165×10^{-5}	0.0815×10^{-5}	0.0557×10^{-5}
	Double (6×10^{-7})	0.1194×10^{-5}	0.0860×10^{-5}	0.0640×10^{-5}
	Half (1.5×10^{-7})	0.1013×10^{-5}	0.0666×10^{-5}	0.03545×10^{-5}
Impulsive reference	——	0.0837×10^{-5}	0.0669×10^{-5}	0.0169×10^{-5}

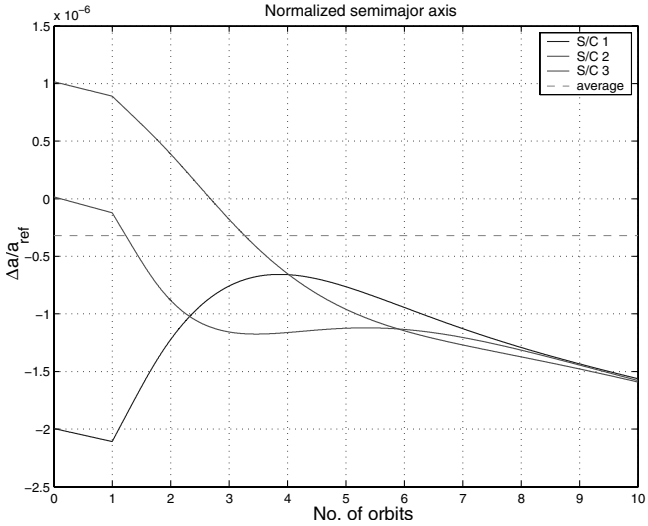

Fig. 12 Semimajor axes of the satellites with the nominal full control law. The whole formation is losing altitude but maintains the same semimajor axis.

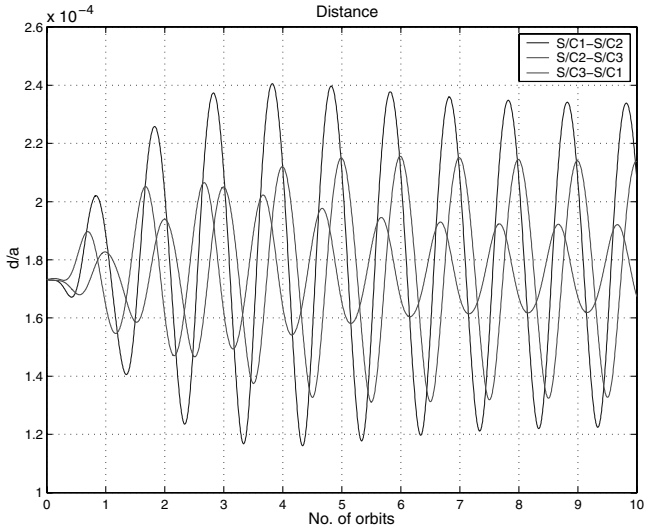

Fig. 13 The relative distances between satellites remain bounded despite drag.

of the satellites, with the nominal full control law, is shown is Fig. 12. It is clear that the whole formation is losing altitude, due to the drag, but the formation stays together, as shown in Fig. 13, since the control law acts to equalize the semimajor axes.

VII. Conclusions

In this work, we have shown that LOS vector measurements are sufficient for guaranteeing stable formations in the sense of energy matching. The main conclusion is, therefore, that if merely bounded relative motion is required, as is the case in many actual missions, existing LOS sensors can be used to generate continuous stabilizing fuel-efficient feedback. Moreover, we have shown that relative range measurement is not necessary. In fact, only the LOS direction is required for feedback stabilization of the formation, although full LOS measurement improves convergence. The stabilization mechanism in both the full and reduced controllers is equalization of the SMAs of the formation flying spacecraft. The common SMA value, however, is not necessarily equal to that of the reference orbit.

An implementation of the LOS-based control formalism facilitates the design of leaderless formations. If every spacecraft in the formation tracks the LOS to its neighboring spacecraft and the last spacecraft tracks again the first spacecraft, a cyclic formation pattern is created. This pattern is robust because it is inherently leaderless. In addition, all initial SMA errors of all formation members are averaged in steady state, and all spacecraft ultimately possess the same SMA which is the centroid of the initial SMAs.

The opposite case is where there is a designated leader which does not track any other spacecraft, but every other spacecraft tracks a neighboring spacecraft to create a (graph theoretic) tree. In this case, all the SMAs of the follower spacecraft will converge to that of the leader, yielding again a stable formation. However, if the initial SMA of the leader is large, considerable maneuver effort, and hence fuel expenditure, will be required to steer all the follower spacecraft to assume the leader's SMA. This phenomenon is inherently prevented in the cyclic topology.

Appendix A: Auxiliary Calculations for Stability Analysis

In this Appendix we prove that

$$\frac{\partial y_j}{\partial a_j}(t, a_{\text{ref}}) - \frac{\partial y_j}{\partial a_j}(t-T, a_{\text{ref}}) < 0$$

The stability analysis is linear; therefore it is consistent to use the linearized equations of motion in the following analysis.

The position components of the linear relative trajectory of some S_i with respect to the reference orbit are obtained by solving the linearized system (10) (for simplicity, we omit the index i):

$$x(t) = -\left(3x_0 + \frac{2}{n}\dot{y}_0\right)\cos nt + \frac{\dot{x}_0}{n}\sin nt + \frac{2}{n}\dot{y}_0 + 4x_0 \tag{A1}$$

$$y(t) = 6(\sin nt - nt)x_0 + y_0 + \frac{2}{n}(\cos nt - 1)\dot{x}_0 + (4\sin nt - 3nt)\frac{\dot{y}_0}{n} \tag{A2}$$

$$z(t) = z_0 \cos nt + \frac{\dot{z}_0}{n}\sin nt \tag{A3}$$

Here $n = n_{\text{ref}}$ is the mean motion of the reference orbit, and x_0, y_0, z_0, $\dot{x}_0$, $\dot{y}_0$, and $\dot{z}_0$ are initial conditions, or, alternatively, constants of integration. From the linear perspective, $a_i \neq a_{\text{ref}}$ due to $\dot{y}_0$ and x_0. To find the relationship between a change in a and the concomitant change in $\dot{y}_0$ and x_0, we differentiate the vis-viva equation written in its Euler–Hill form (9) with respect to the state vector $\boldsymbol{x} = [x, y, z, \dot{x}, \dot{y}, \dot{z}]^T$:

$$\Delta a = -\frac{\mu}{2}\left[\left(\frac{\partial(1/\varepsilon)}{\partial \mathbf{x}}\right)\Bigg|_{\substack{x=y=z=0\\ \dot{x}=\dot{y}=\dot{z}=0}} \Delta \boldsymbol{x}\right] \tag{A4}$$

Equation (A4) gives

$$\frac{\partial}{\partial a} = \frac{n}{2}\frac{\partial}{\partial(\dot{y}_0 + 2nx_0)} \tag{A5}$$

Thus, we can evaluate the partials of x, y, and z with respect to a from their partials with respect to $\dot{y}_0 + 2nx_0$. Subtracting Eqs. (A1–A3) evaluated at t and $t-T$ and differentiating with respect to $\dot{y}_0 + 2nx_0$ yields

$$\frac{\partial x}{\partial a}(t) - \frac{\partial x}{\partial a}(t-T) = 0, \qquad \frac{\partial y}{\partial a}(t) - \frac{\partial y}{\partial a}(t-T) = -\frac{3nT}{2} < 0,$$
$$\frac{\partial z}{\partial a}(t) - \frac{\partial z}{\partial a}(t-T) = 0$$

Appendix B: Stability Analysis of the LOS Bearing-Based Controller

Similar to the derivation in Sec. IV.A, to establish stability of (41) we linearize $\hat{\boldsymbol{\ell}}_i$ about the reference SMA,

$$\hat{\boldsymbol{\ell}}_i(t,a_j,a_i)=\hat{\boldsymbol{\ell}}_i(t,a_{\text{ref}})+\frac{\partial\hat{\boldsymbol{\ell}}_i}{\partial a_j}(t,a_{\text{ref}})\Delta a_j+\frac{\partial\hat{\boldsymbol{\ell}}_i}{\partial a_i}(t,a_{\text{ref}})\Delta a_i \quad \text{(B1)}$$

where

$$\frac{\partial\hat{\boldsymbol{\ell}}_i}{\partial a}=\frac{\partial}{\partial a}\left(\frac{\boldsymbol{\ell}_i}{\ell_i}\right)=\frac{1}{\ell_i}\left[\frac{\partial\boldsymbol{\ell}_{ii}}{\partial a}-\left(\hat{\ell}_i\cdot\frac{\partial\boldsymbol{\ell}_i}{\partial a}\right)\hat{\boldsymbol{\ell}}_i\right] \quad \text{(B2)}$$

The linearized control law is then given by

$$\begin{aligned}\boldsymbol{f}_i=\boldsymbol{f}_{\text{ss}i}&-K\left(\frac{\partial\hat{\boldsymbol{\ell}}_i}{\partial a_j}(t,a_{\text{ref}})-\frac{\partial\hat{\boldsymbol{\ell}}_i}{\partial a_j}(t-T,a_{\text{ref}})\right)\Delta a_j\\&-K\left(\frac{\partial\hat{\boldsymbol{\ell}}_i}{\partial a_i}(t,a_{\text{ref}})-\frac{\partial\hat{\boldsymbol{\ell}}_i}{\partial a_i}(t-T,a_{\text{ref}})\right)\Delta a_i\end{aligned} \quad \text{(B3)}$$

where $\boldsymbol{f}_{\text{ss}i}=-K[\hat{\boldsymbol{\ell}}_i(t,a_{\text{ref}})-\hat{\boldsymbol{\ell}}_i(t-T,a_{\text{ref}})]$. The $\hat{\mathbf{y}}$ component of this force is now substituted into Eq. (20). Expanding and keeping only first-order terms with Δa, we obtain

$$\begin{aligned}\Delta\dot{a}_i=\frac{2}{n_{\text{ref}}}\Bigg[&f_{\text{ss}yi}-K\left(\frac{\partial\hat{\boldsymbol{\ell}}_i}{\partial a_j}(t,a_{\text{ref}})-\frac{\partial\hat{\boldsymbol{\ell}}_i}{\partial a_j}(t-T,a_{\text{ref}})\right)\cdot\hat{\mathbf{y}}\Delta a_j\\&-K\left(\frac{\partial\hat{\boldsymbol{\ell}}_i}{\partial a_i}(t,a_{\text{ref}})-\frac{\partial\hat{\boldsymbol{\ell}}_i}{\partial a_i}(t-T,a_{\text{ref}})\right)\cdot\hat{\mathbf{y}}\Delta a_i\Bigg]\end{aligned} \quad \text{(B4)}$$

The next step is to average the dynamics of the SMAs over one orbital period of the reference orbit. Because $\hat{\boldsymbol{\ell}}_i(t,a_{\text{ref}})-\hat{\boldsymbol{\ell}}_i(t-T,a_{\text{ref}})=0$, the steady-state constituent of the control force, $f_{\text{ss}yi}$, is also zero.

To determine the mean value of the remaining terms, let us first investigate a single term of Eq. (B4). We have

$$\begin{aligned}\frac{\partial\hat{\boldsymbol{\ell}}_i}{\partial a_j}(t,a_{\text{ref}})\cdot\hat{\mathbf{y}}&=\frac{1}{\ell_i}\left[\frac{\partial\boldsymbol{\ell}_i}{\partial a_j}(t,a_{\text{ref}})-\left(\hat{\boldsymbol{\ell}}_i\cdot\frac{\partial\boldsymbol{\ell}_i}{\partial a_j}(t,a_{\text{ref}})\right)\hat{\boldsymbol{\ell}}_i\right]\cdot\hat{\mathbf{y}}\\&=\frac{1}{\ell_i}\left[\frac{\partial\boldsymbol{\ell}_i}{\partial a_j}(t,a_{\text{ref}})\cdot\hat{\mathbf{y}}-\frac{1}{\ell_i^2}\left(\boldsymbol{\ell}_i\cdot\frac{\partial\boldsymbol{\ell}_i}{\partial a_j}(t,a_{\text{ref}})\right)\boldsymbol{\ell}_i\cdot\hat{\mathbf{y}}\right]\\&=\frac{1}{\ell_i}\left[\frac{\partial\ell_{iy}}{\partial a_j}(t,a_{\text{ref}})-\frac{1}{\ell_i^2}\left(\boldsymbol{\ell}_i\cdot\frac{\partial\boldsymbol{\ell}_i}{\partial a_j}(t,a_{\text{ref}})\right)\ell_{iy}\right]\\&=\frac{1}{\ell_i}\left[\frac{\partial y_j}{\partial a_j}(t,a_{\text{ref}})-\frac{1}{\ell_i^2}\left(\boldsymbol{\ell}_i\cdot\frac{\partial\boldsymbol{\ell}_i}{\partial a_j}(t,a_{\text{ref}})\right)\ell_{iy}\right]\end{aligned} \quad \text{(B5)}$$

where $\ell_{iy}\equiv\boldsymbol{\ell}_i\cdot\hat{\mathbf{y}}=y_j-y_i$ is the $\hat{\mathbf{y}}$-component of the LOS vector. Similarly,

$$\frac{\partial\hat{\boldsymbol{\ell}}_i}{\partial a_i}(t,a_{\text{ref}})\cdot\hat{\mathbf{y}}=\frac{1}{\ell_i}\left[-\frac{\partial y_i}{\partial a_i}(t,a_{\text{ref}})-\frac{1}{\ell_i^2}\left(\boldsymbol{\ell}_i\cdot\frac{\partial\boldsymbol{\ell}_i}{\partial a_i}(t,a_{\text{ref}})\right)\ell_{iy}\right] \quad \text{(B6)}$$

Using Eq. (B4) we derive

$$\begin{aligned}\Delta\dot{a}_i=&-\frac{2}{n_{\text{eq}}}\frac{K}{\ell_i}\Bigg[\frac{\partial y_j}{\partial a_j}(t,a_{\text{ref}})-\frac{\partial y_j}{\partial a_j}(t-T,a_{\text{ref}})\\&-\frac{1}{\ell_i^2}\left(\boldsymbol{\ell}_i\cdot\frac{\partial\boldsymbol{\ell}_i}{\partial a_j}(t,a_{\text{ref}})\right)\ell_{iy}+\frac{1}{\ell_i^3}\left(\boldsymbol{\ell}_i\cdot\frac{\partial\boldsymbol{\ell}_i}{\partial a_j}(t-T,a_{\text{ref}})\right)\ell_{iy}\Bigg]\Delta a_j\\&-\frac{2}{n_{\text{eq}}}\frac{K}{\ell_i}\Bigg[-\frac{\partial y_i}{\partial a_i}(t,a_{\text{ref}})+\frac{\partial y_i}{\partial a_i}(t-T,a_{\text{ref}})\\&-\frac{1}{\ell_i^2}\left(\boldsymbol{\ell}_i\cdot\frac{\partial\boldsymbol{\ell}_i}{\partial a_i}(t,a_{\text{ref}})\right)\ell_{iy}\\&+\frac{1}{\ell_i^3}\left(\boldsymbol{\ell}_i\cdot\frac{\partial\boldsymbol{\ell}_i}{\partial a_i}(t-T,a_{\text{ref}})\right)\ell_{iy}\Bigg]\Delta a_i\end{aligned} \quad \text{(B7)}$$

When we compare Eq. (B7) to Eq. (27), we note that there exist extra terms that contain the scalar product $\boldsymbol{\ell}_i\cdot(\partial\boldsymbol{\ell}_i/\partial a)$, and the expansion thereof gives

$$\begin{aligned}&\boldsymbol{\ell}_i\cdot\frac{\partial\boldsymbol{\ell}_i}{\partial a_i}(t,a_{\text{ref}})-\boldsymbol{\ell}_i\cdot\frac{\partial\boldsymbol{\ell}_i}{\partial a_i}(t-T,a_{\text{ref}})\\&=\boldsymbol{\ell}_i\cdot\left[\frac{\partial\boldsymbol{\ell}_i}{\partial a_i}(t,a_{\text{ref}})-\frac{\partial\boldsymbol{\ell}_i}{\partial a_i}(t-T,a_{\text{ref}})\right]\\&=\boldsymbol{\ell}_i\cdot\frac{\partial}{\partial a_j}[\boldsymbol{\ell}_i(t,a_{\text{ref}})-\boldsymbol{\ell}_i(t-T,a_{\text{ref}})]\\&=\ell_{ix}\cdot\frac{\partial}{\partial a_j}[\ell_{ix}(t,a_{\text{ref}})-\ell_{xi}(t-T,a_{\text{ref}})]\\&+\ell_{iy}\cdot\frac{\partial}{\partial a_j}[\ell_{yi}(t,a_{\text{ref}})-\ell_{iy}(t-T,a_{\text{ref}})]\\&+\ell_{zi}\cdot\frac{\partial}{\partial a_j}[\ell_{iz}(t,a_{\text{ref}})-\ell_{zi}(t-T,a_{\text{ref}})]\end{aligned} \quad \text{(B8)}$$

Following the derivation in Appendix A, we have

$$\begin{aligned}&\frac{\partial x_j}{\partial a_j}(t,a_j)-\frac{\partial x_j}{\partial a_j}(t-T,a_j)=0,\\&\frac{\partial z_j}{\partial a_j}(t,a_j)-\frac{\partial z_j}{\partial a_j}(t-T,a_j)=0,\\&\frac{\partial y_j}{\partial a_j}(t,a_j)-\frac{\partial y_j}{\partial a_j}(t-T,a_j)<0\end{aligned} \quad \text{(B9)}$$

These relationships exist for spacecraft i as well. Therefore

$$\begin{aligned}&\boldsymbol{\ell}_i\cdot\frac{\partial\boldsymbol{\ell}_i}{\partial a_i}(t,a_{\text{ref}})-\boldsymbol{\ell}_i\cdot\frac{\partial\boldsymbol{\ell}_i}{\partial a_i}(t-T,a_{\text{ref}})\\&=\ell_{iy}\cdot\frac{\partial}{\partial a_j}[\ell_{yi}(t,a_{\text{ref}})-\ell_{iy}(t-T,a_{\text{ref}})]\end{aligned} \quad \text{(B10)}$$

Substituting (B9) and (B10) into Eq. (B7) entails

$$\begin{aligned}\Delta\dot{a}_i=&-\frac{2}{n_{\text{ref}}}\frac{K}{\ell_i}\Bigg\{\frac{\partial y_j}{\partial a_j}(t,a_{\text{ref}})-\frac{\partial y_j}{\partial a_j}(t-T,a_{\text{ref}})\\&-\frac{\ell_{iy}^2}{\ell_i^2}\left[\left(\frac{\partial\ell_{iy}}{\partial a_j}(t,a_{\text{ref}})\right)-\left(\frac{\partial\ell_{iy}}{\partial a_j}(t-T,a_{\text{ref}})\right)\right]\Bigg\}\Delta a_j\\&-\frac{2}{n_{\text{ref}}}\frac{K}{\ell_i}\Bigg\{-\frac{\partial y_i}{\partial a_i}(t,a_{\text{ref}})+\frac{\partial y_i}{\partial a_i}(t-T,a_{\text{ref}})\\&-\frac{\ell_{iy}^2}{\ell_i^2}\left[\left(\frac{\partial\ell_{iy}}{\partial a_i}(t,a_{\text{ref}})\right)-\frac{1}{\ell_i^3}\left(\frac{\partial\ell_{iy}}{\partial a_i}(t-T,a_{\text{ref}})\right)\right]\Bigg\}\Delta a_i\end{aligned} \quad \text{(B11)}$$

Recalling that $\ell_{iy}(t,a_j,a_i)\equiv\boldsymbol{\ell}_i(t,a_j,a_i)\cdot\hat{\mathbf{y}}=[y_j(t,a_j)-y_i(t,a_i)]$ provides

$$\frac{\partial\ell_{iy}}{\partial a_j}(t,a_{\text{ref}})=\frac{\partial y_j}{\partial a_j}(t,a_{\text{ref}}),\qquad\frac{\partial\ell_{iy}}{\partial a_i}(t,a_{\text{ref}})=-\frac{\partial y_i}{\partial a_i}(t,a_{\text{ref}}) \quad \text{(B12)}$$

Hence

$$\begin{aligned}\Delta\dot{a}_i=&-\frac{2}{n_{\text{ref}}}\frac{K}{\ell_i}\left(1-\frac{\ell_{iy}^2}{\ell_i^2}\right)\Bigg\{\left[\frac{\partial y_j}{\partial a_j}(t,a_{\text{ref}})-\frac{\partial y_j}{\partial a_j}(t-T,a_{\text{ref}})\right]\Delta a_j\\&-\left[\frac{\partial y_i}{\partial a_i}(t,a_{\text{ref}})-\frac{\partial y_i}{\partial a_i}(t-T,a_{\text{ref}})\right]\Delta a_i\Bigg\}\end{aligned} \quad \text{(B13)}$$

Upon averaging, we obtain

$$\Delta\dot{a}_i=-\frac{2}{n_{\text{ref}}}\frac{K}{\overline{\ell}_i}\left(1-\frac{\overline{\ell_{iy}^2}}{\overline{\ell_i^2}}\right)D(\Delta a_j-\Delta a_i) \quad \text{(B14)}$$

where D is defined as in Eq. (29) and $\overline{(\cdot)}$ denotes a time-averaged quantity. This equation can be rewritten into

$$\Delta\dot{a}_i = -\frac{2}{n_{\text{ref}}} K_R D_R (\Delta a_j - \Delta a_i) \tag{B15}$$

where $K_R = K/\overline{\ell}_i$ and $D_R = [1 - (\overline{\ell}_{iy}/\overline{\ell}_i)^2]D$. Clearly, $[1 - (\overline{\ell}_{iy}/\overline{\ell}_i)^2] > 0$, hence $\text{sgn}(D_R) \equiv \text{sgn}(D)$. Equation (42) has the same structure as the equation for the full controller, Eq. (30). The conclusion is then the same, that is, the controller is stable in the sense of (8) for $K > 0$.

Acknowledgments

The contribution of Pini Gurfil was supported by the Robert and Mildred Rosenthal Aerospace Engineering Research Grant. This research was performed while David Mishne was a Visiting Scientist in the Asher Space Research Institute at the Technion—Israel Institute of Technology.

References

[1] Schaub, H., Vadali, S. R., and Alfriend, K. T., "Spacecraft Formation Flying Control Using Mean Orbital Elements," *Journal of the Astronautical Sciences*, Vol. 48, No. 1, 2000, pp. 69–87.

[2] Mishne, D., "Formation Control of Satellites Subject to Drag Variations and J_2 Perturbations," *Journal of Guidance, Control, and Dynamics*, Vol. 27, No. 4, 2004, pp. 685–692.

[3] Gurfil, P., "Relative Motion between Elliptic Orbits: Generalized Boundedness Conditions and Optimal Formationkeeping," *Journal of Guidance, Control, and Dynamics*, Vol. 28, No. 4, July 2005, pp. 761–767.

[4] Schaub, H., and Alfriend, K., "Hybrid Cartesian and Orbit Elements Feedback Law for Formation Flying Spacecraft," *Journal of Guidance, Control, and Dynamics*, Vol. 25, No. 2, March–April 2002, pp. 387–393.

[5] Gurfil, P., Idan, M., and Kasdin, N. J., "Adaptive Neural Control of Deep-Space Formation Flying," *Journal of Guidance, Control, and Dynamics*, Vol. 26, No. 3, May 2003, pp. 491–501.

[6] Yeh, H. H., Nelson, E., and Sparks, A., "Nonlinear Tracking Control for Satellite Formations," *Journal of Guidance, Control, and Dynamics*, Vol. 25, No. 2, March–April 2002, pp. 376–386.

[7] Inalhan, G., Tillerson, M., and How, J. P., "Relative Dynamics and Control of Spacecraft Formations in Eccentric Orbits," *Journal of Guidance, Control, and Dynamics*, Vol. 25, No. 1, Jan. 2002, pp. 48–60.

[8] Mesbahi, M., and Hadaegh, F. Y., "Formation Flying Control of Multiple Spacecraft via Graphs, Matrix Inequalities and Switching," *Journal of Guidance, Control, and Dynamics*, Vol. 24, No. 2, March 2001, pp. 369–377.

[9] Busse, F., and How, J. P., "Real-time Experimental Demonstration of Precise Decentralized Relative Navigation for Formation Flying Spacecraft," *AIAA Guidance, Navigation, and Control Conference*, AIAA, Reston, VA, Aug. 2002.

[10] Rogers, A., Anderson, K., Mracek, A., Zenick, A., Grau, J., and Gramling, C., "An Integrated Vision-Based System for Spacecraft Attitude Topology Determination for Formation Flying Missions," AIAA Paper SSC04-IV-2, 2004.

[11] Behroozi, F., and Gagnon, R., "Cyclic Pursuit in a Plane," *Journal of Mathematical Physics*, Vol. 20, No. 11, 1979, pp. 2212–2216.

[12] Bruckstein, A. M., "Why the Ant Trails Look So Straight and Nice," *The Mathematical Intelligencer*, Vol. 15, No. 2, 1993, pp. 58–62.

[13] Marshal, J. A., and Broucke, M. E., "Formations of Vehicles in Cyclic Pursuit," *IEEE Transactions on Automatic Control*, Vol. 49, No. 11, Nov. 2004, pp. 1963–1974.

[14] Diestel, R., *Graph Theory*, Springer–Verlag, New York, 2005.

[15] Davis, P. J., *Circulant Matrices*, American Mathematical Society, Providence, RI, 1994.

[16] Lafferriere, G., Caughman, J., and Williams, A., "Graph Theoretic Methods in the Stability of Vehicle Formations," *Proceedings of the 2004 American Control Conference*, 2004, pp. 3729–3724.

[17] Clohessy, W. H., and Wiltshire, R. S., "Terminal Guidance System for Satellite Rendezvous," *Journal of the Astronautical Sciences*, Vol. 27, No. 9, Sept. 1960, pp. 653–678.

[18] Battin, R. H., *An Introduction to the Mathematics and Methods of Astrodynamics*, AIAA, Reston, VA, 1999, pp. 485–488, Chap. 10.